Spatial structure of the M2 transmembrane segment of the nicotinic acetylcholine receptor α-subunit

Vladimir S. Pashkov, Innokenty V. Maslennikov, Leonid D. Tchikin, Roman G. Efremov, Vadim T. Ivanov, Alexander S. Arseniev*

Shemyakin-Ovchinnikov Institute of Bioorganic Chemistry, Russian Academy of Sciences, 16/10 Miklukho-Maklaya, Moscow 117871, Russia

Received 23 April 1999

Abstract A synthetic peptide corresponding to the transmembrane segment M2 (residues 236–267) of the α-subunit of the nicotinic acetylcholine receptor from *Torpedo californica* has been studied by two dimensional ^{1}H-NMR spectroscopy in a chloroform-methanol (1:1) mixture containing 0.1 M $LiClO_4$. Reconstruction of the spatial structure of M2 from the NMR data resulted in an α-helix formed by residues 241–263. Distribution of the molecular hydrophobicity potential on the helix surface is very similar to that in five-helix bundles of proteins with a known three dimensional structure: two hydrophilic bands located on the opposite helix sides separated by strong hydrophobic zones.

Key words: Nicotinic acetylcholine receptor; Membrane domain; NMR; Conformational analysis

1. Introduction

The nicotinic acetylcholine receptor (nAChR) is one of the best-characterized neurotransmitter-gated ion channels (see recent review [1]). nAChR of *Torpedo californica* consists of four different subunits with an $\alpha_2\beta\gamma\delta$ stoichiometry (50, 54, 56, 58 kDa, respectively). Each of the subunits contains four segments (M1–M4) which are thought to transverse the membrane [2]. There are sequence similarities between M1–M4 segments of the different subunits. According to the affinity labelling experiments [3,4], segments M1, M3 and M4 are in contact with the lipids, while segment M2 is shielded from them. Analysis of electron microscopic images of the transmembrane (TM) part of the nAChR channel in open and closed states, obtained at 0.9 nm resolution [5], indicate that the funnel-shaped ion pore is lined by five helical segments that are arranged symmetrically around the central pore and are kinked about their mid-points. It has been proposed [5] that the helices are formed by M2 segments, one from each subunit, and that the channel opening gate is formed by the side chains of L-251 located at the helix kinks. The results of investigation of reactivities of single cysteine-substituted mutants of α-subunit were considered as an indication that the M2 segment forms an α-helix interrupted by an extended structure from L-250 to S-252 [6] and that the channel opening gate is formed by the residues G-240–T-244 [7]. On the other hand, a NMR study of the M2 segment of the δ-subunit incorporated into phospholipid bilayers or dodecylphosphocholine micelles did not reveal any distortion of the central part of M2 helix [8].

In order to obtain additional insight into the structure and function of the nAChR, molecular modeling studies of the nAChR ion pore have been undertaken. These studies were based on the electron microscopy, mutagenesis and affinity labelling data of nAChR as well as on available structures of the five-helix bundle proteins (for recent reviews, see [9,10]). The elaborated models provide an explanation for a number of results obtained in labelling and mutation studies of nAChR as well as the channel conductance, but, as mentioned in [9], better structural data are required to evaluate such models.

The present communication describes the spatial structure of the M2 segment of the α-subunit of nAChR *T. californica* determined by means of ^{1}H-NMR spectroscopy. Its primary structure differs by 48% from that of the δ-subunit of nAChR studied by NMR [8]. Since the M2 segments of the receptor are deprived of contacts with lipids [3,4], we used a mixture of organic solvents (chloroform/methanol = 1/1 containing 0.1 M $LiClO_4$) instead of detergent micelles. The chloroform/methanol mixture produces a microheterogeneous environment of solvated amphiphilic molecules [11] which should be adequate for the M2 segment with its non-lipid surroundings in the intact nAChR. This medium was successfully used in elucidation of the spatial structure and dynamics of bacteriorhodopsin and its fragments [12,13], of the c subunit of F1F0 ATPase [14], as well as of the multidrug transporter EmrE [15].

2. Materials and methods

The synthetic M2 fragment corresponding to residues 236–267 of the α-subunit of nAChR *T. californica* was prepared by standard solid-phase techniques on a Beckman 990 synthesizer. Methionine residue 243, presented in nAChR, was substituted by norleucine. Such an isosteric replacement usually does not affect the peptide conformation [16], while simplifying the synthesis. In addition, T-267 was amidated. The peptide was purified on Ultrasphere-octyl and Vydak C4 high performance liquid chromatography (HPLC) preparative scale columns. Its purity was confirmed by amino acid analysis and reverse-phase HPLC.

NMR samples were prepared by solubilizing 5.5 mg M2 in 0.6 ml of chloroform/methanol = 1/1 containing 0.1 M $LiClO_4$. CD_3OH (99% deuterium, Isotope, Russia), CD_3OD (99.5% deuterium, Stohler Isotope Chemicals) and $CDCl_3$ (100% deuterium, Stohler Isotope Chemicals) have been used. ^{1}H-NMR spectra were obtained using the Varian Unity 600 (600 MHz) spectrometer at 30°C. Double-quantum-filtered COSY (DQF-COSY), TOCSY (mixing times of 30 and 80 ms) and 100 and 200 ms NOESY spectra of M2 were taken using

*Corresponding author. Fax: (7) (095) 335-50-33.
E-mail: aars@nmr.ru

Abbreviations: nAChR, nicotinic acetylcholine receptor; DQF-COSY, double-quantum-filtered COSY; NOE, nuclear Overhauser effect; MHP, molecular hydrophobicity potential; TM, transmembrane

0014-5793/99/$20.00
PII: S0014-5793(99)01023-6

the WATERGATE scheme [17] for the suppressing of the methanol OH resonance by Z-gradient pulses. A relaxation delay of 1.4 s was used. To measure deuterium exchange rates of the amide protons, the six consecutive 80 ms TOCSY spectra of M2 $CDCl_3/CD_3OD = 1/1$ with 0.1 M $LiClO_4$ were recorded (6.5 h per spectrum).

The XEASY program [18] was applied for analysis of the NMR spectra and measurements of the cross-peak volumes. Spin-spin coupling constants $^3J_{N\alpha}$ were determined from the cross-sections along the ω_2 axis of the non-overlapping NOESY cross-peaks using the INFIT program [19]. Spin-spin coupling constants $^3J_{\alpha\beta}$ were estimated by measuring splittings of the corresponding cross-peaks in the DQF-COSY and NOESY spectra.

Preliminary calculations of the M2 spatial structure were executed using the program DYANA [20] on the basis of the upper limit interproton distance and the dihedral angle constraints which were calculated from the NOESY cross-peak volumes and the vicinal spin-spin coupling constants using HABAS and CALIBA programs of the program package DYANA.

Calculation of lower interproton distance constraints and refinement of the upper ones were carried out by the proton relaxation matrix analysis program MARDIGRAS [21] using a structure generated by the preliminary DYANA calculations and the NOESY cross-peak volumes. The MARDIGRAS-derived set of distance constraints along with the dihedral angle constraints were used to re-calculate the M2 spatial structure by the program DYANA. The M2 structures obtained were then subjected to constrained energy refinement using the ECEPP/2 potential implemented in the program FANTOM [22]. To maintain the structures in conformity with the experimental data, pseudo-energy terms were introduced for distance and dihedral angle constraints with the pseudo-force-field constants of 5.78×10^9 kT nm^{-1} and kT/2 $degree^{-1}$, respectively. The moderately polar environment of M2 was mimicked using an implicit solvation model based on the formalism of atomic solvation parameters for octanol-water transfer [23]. After 3000 steps of conjugate gradients energy minimization, 20 lowest-energy structures were selected to represent the M2 spatial structure.

Analysis of the structure and some art works were performed using the program MOLMOL [24]. The hydrogen bonds were assessed using standard conditions (O...H distance < 0.24 nm, O...H-N angle 145–180°). Hydrophobic properties of the M2 helical segment were calculated for the structure with the minimal conformational energy using the molecular hydrophobicity potential (MHP) approach as described elsewhere [25].

3. Results and discussion

The complete proton resonance assignment of M2 was obtained using standard methods [26] on the basis of DQF-COSY, TOCSY and NOESY spectra. A summary of the experimental NMR data outlining the secondary structure of M2 is presented in Fig. 1.

327 Cross-peaks of different proton pairs were identified and integrated in the NOESY spectra of M2 and stereospecific assignments of 16 diastereotopic pairs were established at the end of the preliminary determination of the spatial structure by the program DYANA. After calculation of the lower interproton distance constraints and refinement of the upper ones using the program MARDIGRAS, 193 upper and 116 lower meaningful interproton distance constraints were obtained. These constraints, along with 34 dihedral angle constraints (24 and 10 for ϕ and χ^1 angles, respectively) generated from the values of vicinal spin-spin coupling constants $^3J_{HN-C\alpha H}$ and $^3J_{C\alpha H-C\beta H}$, were used in DYANA calculations of the spatial structure. To avoid mistakes in a choice of hydrogen bond acceptors, the deuterium exchange data of amide hydrogens were not employed as constraints used in further calculations.

Of the 20 best DYANA structures (out of the 300 calculated), some have an unfavorable conformational energy and comparatively high values of van der Waals constraint violations (Table 1). To improve these undesirable results, the DYANA structures were subjected to constrained energy refinement using the FANTOM program. As a result, a moderate increase of experimental constraint violations occurred, whereas the values and the dispersion of the potential energy and van der Waals constraint violations were significantly reduced (Table 1). The resulted set of 20 best FANTOM structures of M2 is shown in Fig. 2 and the corresponding dihedral angles are depicted in Fig. 3.

As seen in Figs. 2 and 3, the conformations of N- and C-terminal parts of M2 (residues P-236–G-240 and S-266–T-267, respectively) are not defined. This is in agreement with the averaged values of spin-spin coupling constants $^3J_{N\alpha}$ and the fast exchange of the amide protons in the terminal parts (Fig. 1). The polypeptide chain of all 20 best M2 structures forms a right-handed α-helix which extends from E-241 to L-263, where mean pairwise RMSDs of the backbone and of all heavy atoms are 0.03 and 0.11 nm, respectively. Assessment of hydrogen bonds revealed that the standard α-helical hydrogen

Fig. 1. Summary of NMR data defining the secondary structure of M2: $d_{AB}(i,j)$, nuclear Overhauser effect (NOE) connectivities between the proton types A and B located in amino acid residues i and j, respectively. Strip heights are proportional to the NOE values. H-D exch., characteristics of the deuterium exchange rates of the amide hydrogens. The amide protons whose cross-peaks observed in the TOCSY spectra started at < 13, 13–26 and > 26 h after M2 dissolving in $CD_3OD/CDCl_3 = 1/1$ containing 0.1 M $LiClO_4$ are shown by thin, intermediate and thick strips, respectively. $^3J_{\alpha N}$, vicinal spin-spin coupling constants between the $C^{\alpha}H$ and HN protons are shown by thin, intermediate and thick strips (< 5.5, 5.5–7.5 and > 7.5 Hz, respectively). Circles stand for the data that could not be measured due to the overlapping cross-peaks.

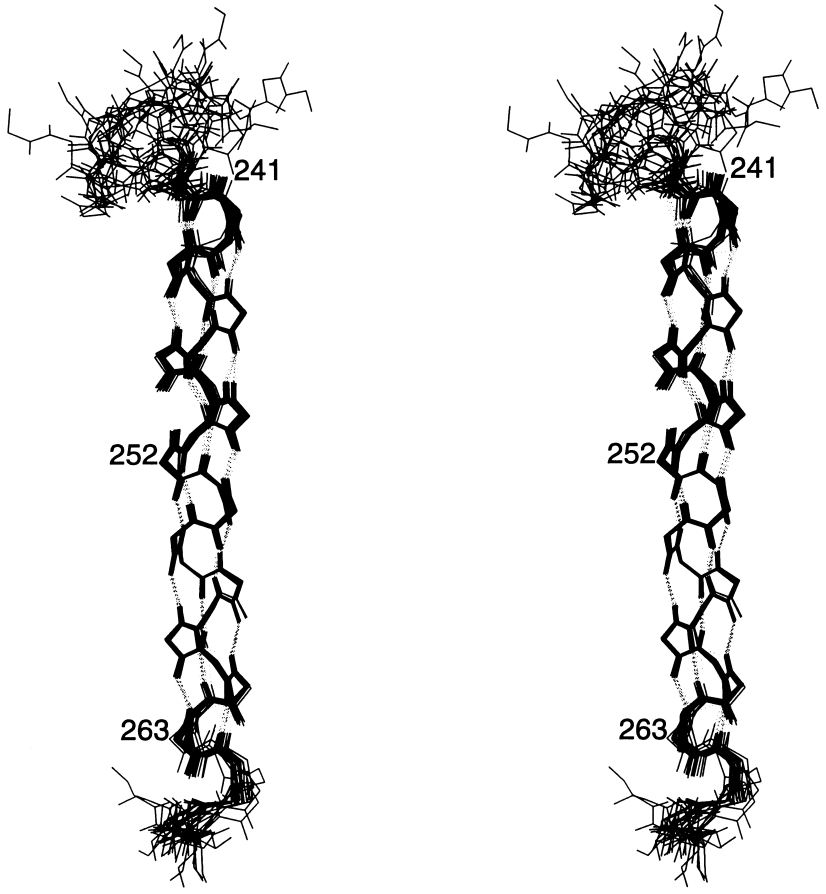

Fig. 2. Stereoview of the 20 best FANTOM structures of M2 aligned by superimposing the backbone atoms of the 241–263 amino acid residues. Numbers show the positions of the C^{α} atoms of E-241, S-252 and L-263. The backbone is shown in solid lines and consistent hydrogen bonds are shown in dotted lines.

bond pattern, CO(*i*)...HN(*i*+4), occurs in most of the 20 structures. One exception is provided by the hydrogen bond between CO S-248 and NH S-252 that was not detected in any of the structures shown in Fig. 2. In this connection, it is worthwhile to mention the low field position of the L-251 NH proton signal which is shifted by more then 0.5 ppm from the rest of the NH proton signals. The absence of the S-248 CO...NH S-252 hydrogen bond results in a local distortion of the helix structure. This finding is in line with the electron microscopy and substituted cysteine accessibility data [5,6], indicating that the M2 helices of nAChR are distorted near L-251. The distorted helix also fits the structure obtained

Table 1
Characteristics of the 20 best DYANA and FANTOM structures of the TM segment M2

Parameter, units	Quantity	DYANA	FANTOM
Target function, nm^2		0.012 ± 0.004	
Number of distance constraints upper/lower		193/116	193/116
Number of dihedral angle constraints	ϕ	24	24
	χ^1	10	10
Upper distance constraint violations, nm	Sum	0.47 ± 0.04	0.54 ± 0.04
	Maximum	0.02 ± 0.01	0.03 ± 0.01
Lower distance constraint violations, nm	Sum	0.25 ± 0.03	0.27 ± 0.04
	Maximum	0.02 ± 0.01	0.02 ± 0.01
Van der Waals constraint violations, nm	Sum	0.15 ± 0.05	0.05 ± 0.02
	Maximum	0.02 ± 0.01	0.01 ± 0.01
Dihedral angle constraint violations, °	Sum	6.7 ± 3.4	7.2 ± 3.6
	Maximum	3.3 ± 1.1	3.6 ± 1.3
RMSD of heavy atom coordinates (residues), nm	Backbone (E-241–L-263)	0.03 ± 0.02	0.03 ± 0.01
	All atoms (E-241–L-263)	0.11 ± 0.02	0.11 ± 0.02
	Backbone (E-241–L-250)	0.03 ± 0.01	0.03 ± 0.02
	Backbone (L-252–L-263)	0.01 ± 0.01	0.01 ± 0.01
Energy, kJ/mol	Total	-155 ± 362	-401 ± 121

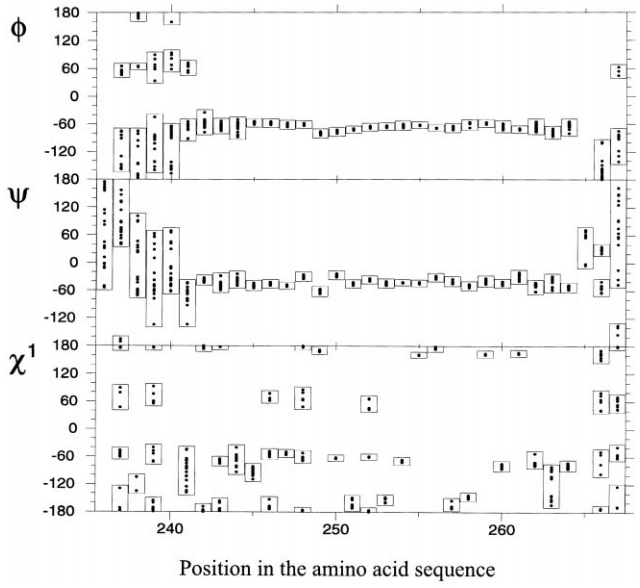

Fig. 3. Scatter plots of φ, ψ and χ^1 angles of the 20 best FANTOM structures of M2.

by molecular modelling [27], where the ion channel looks like a funnel expanding towards the synaptic end formed by the C-terminal parts of the M2 segments.

Analysis of the χ^1 angles (Fig. 3) shows that single rotamers are observed for the bulky side chains of the helix. The only exception is X-243 located at the N-terminus. Several χ^1 rotamers observed for serines 246, 248 and 252 are typical of these small residues in α-helices [28].

The side chain hydroxyls of serine and threonine residues could form hydrogen bonds with the backbone carbonyls, thus competing with backbone NH hydrogens. Signals of the side chain hydroxyls were not detected in the NMR spectra of M2, suggesting thereby that the permanent hydrogen bonds involving these groups are absent. This finding is in agreement with the results of hydrogen bond analysis in the best M2 structures. Two most commonly encountered hydrogen bonds (T-254 OH...OC L-250 and S-252 OH...OC S-248) were found in 45% and 30% of the structures, respectively. Other side chain hydroxyls form hydrogen bonds with a lower occurrence. It seems likely that these temporary hydrogen bonds destabilize the helix resulting in the lack of the S-248 CO...HN S-252 hydrogen bond and the increased dispersion of the structures observed for the N-terminal half of the helix (Table 1 and Fig. 2).

According to the results of affinity labelling experiments [3,4] and electron microscopy date [5], five M2 segments from different subunits of nAChR are arranged pseudo-symmetrically so that each M2 segment faces the polar channel pore, the neighboring M2 segments and other TM segments of nAChR. Obviously, the M2 surface should offer specific properties appropriate to the dislocation. The polarity properties of the surface of the best FANTOM structure were analyzed using the MHP method [25]. A two dimensional (2D) MHP map of the M2 helical region (Fig. 4, top) and especially its projection on the *X*-axis (Fig. 4, bottom) clearly demonstrate two polar regions ($40° < \alpha < 130°$ and $210° < \alpha < 320°$) that are separated by two hydrophobic stretches spanning the whole length of the helix. Interestingly, residues E-241, T-244, S-248, S-252 and E-262, that were supposed [6] to line the ion pore, correspond exactly to the most polar stretch ($40° < \alpha < 130°$, Fig. 4). Hydrophobic interfaces between M2 segment and other components constituting the nAChR ion channel could also be delineated. The interfaces are formed by amino acid residues I-247, L-251, V-255, L-258 ($130° < \alpha < 210°$) and L-245, V-249, L-253, F-256, L-257, I-260, L-263 ($\alpha = 0° \pm 40°$, Fig. 4). It is worthwhile noting that the pattern of the M2 surface (Fig. 4) resembles those observed for the five-helix bundle proteins and clearly differs from that of the four-helix bundle [29].

The spatial structure of the M2 TM segment of nAChR obtained by NMR spectroscopy in the chloroform/methanol mixture containing 0.1 M $LiClO_4$ correlates well with the M2 structure in nAChR revealed by electron microscopy [5] and the substituted cysteine accessibility method [6]. The use of this experimental structure rather than the previously suggested models will allow for more precise modeling of the nAChR ion channel and will hopefully provide an additional insight in the understanding of its functioning.

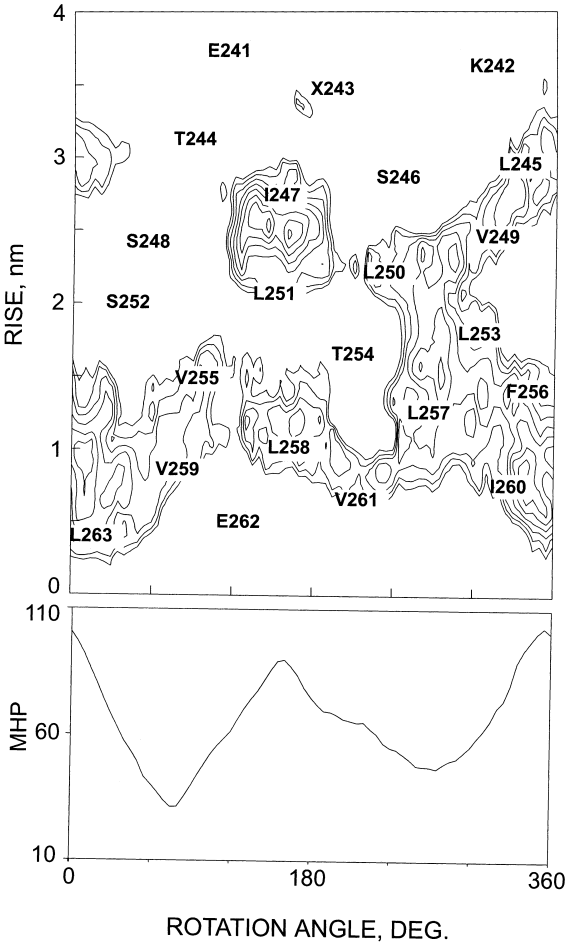

Fig. 4. Hydrophobic properties of the α-helical segment 241–263 of M2. (Top) 2D isopotential map of the MHP on the peptide surface. The rotation angle characterizes rotation about the α-helix axis, RISE is a distance along the helix axis. Only the areas with MHP > 0.1 are shown. Contour intervals are 0.015. The residue positions are indicated by letters. (Bottom) Angular distribution of MHP on the peptide surface.

Acknowledgements: This work was supported in part by RFBR (Grants 97-04-48655 and 98-04-48823).

References

[1] Hucho, F., Tsetlin, V.I. and Machold, J. (1996) Eur. J. Biochem. 239, 539–557.
[2] Finer-Moore, J. and Stroud, R.M. (1984) Proc. Natl. Acad. Sci. USA 81, 155–159.
[3] Blanton, M.P. and Cohen, J. (1994) Biochemistry 33, 2859–2872.
[4] White, B.H. and Cohen, J. (1992) J. Biol. Chem. 267, 15770–15783.
[5] Unwin, N. (1995) Nature 373, 37–43.
[6] Akabas, M.H., Kaufmann, C., Archdeacon, P. and Karlin, A. (1994) Neuron 13, 919–927.
[7] Wilson, G.G. and Karlin, A. (1998) Neuron 20, 1269–1281.
[8] Opella, S.J., Gessel, J., Valente, A.P., Marassi, F.M., Oblatt-Montal, M., Sun, W., Ferrer-Montiel, A. and Montal, M. (1997) Chemtracts - biochemistry and molecular biology 10, 153–174.
[9] Sansom, M.S.P. (1998) Curr. Opin. Struct. Biol. 8, 237–244.
[10] Sansom, M.S., Adcock, C. and Smith, G.R. (1998) J. Struct. Biol. 121, 246–262.
[11] Gratias, R. and Kessler, H. (1998) J. Phys. Chem. (in press).
[12] Maslennikov, I.V., Bocharov, E.V. and Arseniev, A.S. (1995) Bioorg. Khim. 21, 659–674.
[13] Orekhov, V.Y., Pervushin, K.V., Korzhnev, D.M. and Arseniev, A.S. (1995) J. Biomol. NMR 6, 113–122.
[14] Girvin, M.E. and Fillingame, R.H. (1994) Biochemistry 33, 665–674.
[15] Schwaiger, M., Lebendiker, M., Yerushalmi, H., Coles, M., Gröger, A., Schwarz, C., Schuldiner, S. and Kessler, H. (1998) Eur. J. Biochem. 254, 610–619.
[16] Wunsch, E., Moroder, L., Gillessen, D., Sørensen, U.B. and Bali, J.P. (1982) Phisiol. Chem. 363, 665–669.
[17] Piotto, M., Saudek, V. and Sclenář, V. (1992) J. Biomol. NMR 2, 661–665.
[18] Bartels, C., Xia, T.-H., Billeter, M., Günter, P. and Wüthrich, K. (1995) J. Biomol. NMR 5, 1–10.
[19] Szypersky, S. (1992) J. Biol. NMR 2, 432–440.
[20] Günter, P., Mumenthaler, C. and Wüthrich, K. (1997) J. Mol. Biol. 273, 283–298.
[21] Liu, H., Spielmann, H.P., Ulyanov, N.B., Wemmer, D.E. and James, T.L. (1995) J. Biomol. NMR 6, 390–402.
[22] Schaumann, T., Braun, W. and Wüthrich, K. (1990) Biopolimers 29, 679–694.
[23] Nolde, D.E., Arseniev, A.S., Vergoten, G. and Efremov, R.G. (1998) J. Biomol. Struct. Dyn. 15, 1–18.
[24] Karadi, R., Billeter, M. and Wüthrich, K. (1996) J. Mol. Graph. 14, 51–55.
[25] Efremov, R.G. and Vergoten, G. (1995) J. Phys. Chem. 99, 10658–10666.
[26] Clore, G.M. and Gronenborn, A.M. (1991) Prog. NMR Spectrosc. 23, 43–92.
[27] Tikhonov, D.B. and Zhorov, B.S. (1998) Biophys. J. 74, 242–255.
[28] McGregor, M.J., Islam, S.A. and Sternberg, M.J.E. (1987) J. Mol. Biol. 198, 295–310.
[29] Efremov, R.G., Vergoten, G. and Arseniev, A.S. (1999) Theor. Chem. Acc. 101, 73–76.